crystals

MDPI

Article

Comparison of the Electrochemical Performances of Solid Oxide Fuel Cells with Sputtered Thin Barrier Layers Fueled by Hydrogen or Ammonia

Nunzia Coppola [1], Bertrand Morel [2], Giovanni Carapella [3], Dario Montinaro [4], Alice Galdi [1], Hafiz Sami Ur Rehman [5], Pierpaolo Polverino [5], Cesare Pianese [5], Julie Mougin [2] and Luigi Maritato [1,*]

1 Dipartimento di Ingegneria Industriale-DIIN, Università Degli Studi di Salerno and CNR-SPIN, 84084 Fisciano, SA, Italy; ncoppola@unisa.it (N.C.); agaldi@unisa.it (A.G.)
2 CEA/LITEN, Université Grenoble Alpes, 17 rue des Martyrs, CEDEX 9, 38054 Grenoble, France; bertrand.morel@cea.fr (B.M.); julie.mougin@cea.fr (J.M.)
3 Dipartimento di Fisica "E.R. Caianiello", Università Degli Studi di Salerno and CNR-SPIN, 84084 Fisciano, SA, Italy; giocar@sa.infn.it
4 SolydEra S.p.A., 38017 Mezzolombardo, TN, Italy; dario.montinaro@solydera.com
5 Dipartimento di Ingegneria Industriale-DIIN, Università Degli Studi di Salerno, 84084 Fisciano, SA, Italy; hsamiurrehman@unisa.it (H.S.U.R.); ppolverino@unisa.it (P.P.); pianese@unisa.it (C.P.)
* Correspondence: lmaritato@unisa.it; Tel.: +39-089-968267

Abstract: We investigated the influence of a fuel change from pure hydrogen to a hydrogen–ammonia mixture at different percentages on the electrochemical behavior of 50 mm in diameter Solid Oxide Fuel Cells (SOFCs) with sputtered thin buffer layers of Gd-doped ceria, varying the working temperatures from 800 °C to 650 °C. The results show that the performances of the cells are not affected by the fuel change for high working temperatures (800 °C and 750 °C). As an example, a power density value of 802 mW·cm^{-2} at 1 A·cm^{-2} is found when directly feeding the cell with 8 NmL·min^{-1}cm^{-2} of ammonia and with an equivalent flowrate of 12 NmL·min^{-1}cm^{-2} of H_2. These power density output values are higher than those obtained in industrial state-of-art (SoA) SOFCs with screen-printed buffer layers fed with equivalent hydrogen flowrates, thanks to the improved electrochemical performances obtained in the case of cells with sputtered thin buffer layers of Gd-doped ceria. At lower working temperatures (700 °C and 650 °C), slight changes in the electrochemical behavior of the cells are observed. Nevertheless, in this temperature range, we also obtain an output current density value of 0.54 A·cm^{-2} in a pure ammonia flowrate of 12 NmL min^{-1}cm^{-2} at 800 mV and 700 °C, equal to the value observed in SoA button cells with industrial screen-printed GDC barrier layer fueled with 16 NmL·min^{-1}cm^{-2} of H_2. These results pave the way towards the use of innovative SOFC structures with sputtered thin buffer layers fueled by ammonia.

Keywords: ammonia; SOFC; direct ammonia feeding; sputtered barrier layer

Citation: Coppola, N.; Morel, B.; Carapella, G.; Montinaro, D.; Galdi, A.; Ur Rehman, H.S.; Polverino, P.; Pianese, C.; Mougin, J.; Maritato, L. Comparison of the Electrochemical Performances of Solid Oxide Fuel Cells with Sputtered Thin Barrier Layers Fueled by Hydrogen or Ammonia. *Crystals* **2023**, *13*, 1040. https://doi.org/10.3390/cryst13071040

Academic Editors: Fengyu Shen and Yucun Zhou

Received: 2 June 2023
Revised: 27 June 2023
Accepted: 28 June 2023
Published: 29 June 2023

1. Introduction

The urgent need for renewable, sustainable and efficient energy production solutions able to replace fossil fuels in industrial processes has brought attention to hydrogen and hydrogen-related technologies, nowadays considered among the most promising alternatives to fossil-fuel-related energy production. However, hydrogen production is still heavily dependent on fossil fuels, since the main processes are gasification, methane steam reforming and partial oxidation [1,2]. Moreover, limits to the direct utilization of hydrogen come from low energy storage, along with a lack of infrastructures [1,2]. For all these reasons, the interest in alternative hydrogen-carrier fuel is rising and, among them, ammonia seems to be the most attractive candidate, due to its higher gravimetric H_2 content (17.7 wt% in liquid ammonia) when compared with other hydrogen-carrier compounds

(e.g., 13 wt% in methanol and 7 wt% in cyclohexane). Moreover, ammonia is relatively simple to liquify (boiling point −33.4 °C), has a characteristic and well-recognizable smell [3] and its industrial production process, based on the Haber–Bosch reaction, is well-known and simple [4].

Among hydrogen-based electricity production devices, Solid Oxide Fuel Cells (SOFCs) are attractive mainly for their high fuel–current conversion efficiency and their fuel flexibility [5–7]. SOFCs main reaction being based on hydrogen and oxygen ion formation, respectively, at the anode and cathode side, the use of alternative hydrogen-carrie fuels strongly depends on the fuel dissociation reaction efficiency at the anode sides. The use of NH_3 for direct SOFC feeding is favored by the observation that the cracking reaction of ammonia (namely its dissociation in hydrogen and nitrogen) is catalyzed by nickel-based compounds [8,9] which are, actually, the most common materials used as anodes in SOFCs [3,10–13]. Moreover, this cracking reaction being endothermic, the heat management of ammonia-fed SOFC systems could be simplified. On the other hand, limits to direct ammonia feeding to SOFCs are posed by the operating temperature dependence of their decomposition at the anode side. In fact, it was demonstrated [2,9] that cracking reaction efficiency in the presence of nickel-based catalysts, and thus efficient current generation in the SOFC, is limited to the high operating temperatures of the device, with significant performance reductions for temperatures lower than 750 °C.

Recently, with the aim of increasing industrial SoA SOFCs performances in the Intermediate Temperature (IT) range [14,15], physical vapor deposition (PVD) techniques were proposed [16–18] to fabricate the air electrode/electrolyte gadolinia-doped ceria (GDC) barrier layer. Given its long-term expertise in thin film deposition with different PVD techniques (molecular beam epitaxy [19], pulsed laser deposition [20] and sputtering [21], among others), together with their long-time knowledge on the impedance characterization of thin films [22], a research group at the University of Salerno recently proposed an innovative deposition process for the fabrication of GDC thin barrier layers, based on room-temperature radio-frequency (RF) sputtering followed by in-air annealing at moderate temperatures. Huge increments in the output current of hydrogen-fed SOFCs with sputtered GDC layers have been observed with respect to SoA industrial devices [23], both in button cells (up to +78%) [23,24] and in large industrial-scale cells [25–27].

In this work, we investigated the performances, in terms of j-V and electrochemical impedance spectroscopy (EIS), of 5 cm diameter SOFC button cells, in which the barrier layer is room-temperature sputter-deposited and in-air-annealed when they are fed with ammonia at different temperatures in the range of 650–800 °C. By feeding the cell with ammonia–hydrogen mixtures with different percentages of ammonia, we found, at high temperatures (760–800 °C), power density output values higher than those obtained in industrial state of art (SoA) SOFCs with screen-printed buffer layers fed with equivalent hydrogen flowrates. In the temperature range from 700 °C to 650 °C, we observed output current density values in pure ammonia flowrate practically equal to the values obtained in SoA button cells with higher flowrates of H_2. These results indicate the possibility to employ the SOFC structures with sputtered thin buffer layers using pure ammonia as fuel.

2. Materials and Methods

A 400 nm GDC thin film is grown on 5 cm diameter anode/electrolyte half button cell (SolydEra S.p.A., Pergine, Italy) by means of RF magnetron sputtering (MRC RF-Sputtering, Electron Mec Company, Milan, Italy) using a circular $Gd_{0.1}Ce_{0.9}O_{2-\delta}$ sputtering target (Testbourne, Whitchurch, UK, 99.999% purity) with a diameter of 150 mm. The anode/electrolyte half cell consists of 8 µm 8YSZ electrolytes supported on 260 µm Ni/YSZ anodes. The deposition took place at room temperature; thus, oxygen stoichiometry and thin-film granularity were optimized by means of postgrowth annealing [23,24]. Typical deposition parameters are 400 W of power applied at 13 MHz and 2.2 mTorr of process gas (Ar) pressure, producing deposition rates of about 30 nm/min [24]. The buffer layer is then covered at SolydEra S.p.A. with a circular screen-printed cathode, with cathode

inks prepared by mixing the ceramic powders with a terpineol-based vehicle. After screen printing, the layers are sintered at ca. 1100 °C for 2 h [24], thus completing the button cell structure with a final 9 cm^2 active area of the SOFC. In [24], a schematic of the complete sputter-deposited cell is shown.

Electrochemical tests were carried out using one of the testing benches present at the CEA/LITEN research center (Grenoble, France). The anode side of the cell is placed on a current collector made of a nickel grid with 100 mesh·cm^{-2} placed in a Crofer housing setup; the cell is then sealed with glass paste to ensure complete gas tightness of the fuel chamber. On top of the cell, at the cathode side, a gold grid current collector of 100 mesh·cm^{-2} is placed. To complete the cell mounting, a gas diffusor with a 414 g·cm^{-2} weight is placed on the gold current collector in order to enhance the electrical contacts through a mechanical pressure. Once the cell is mounted, the setup is placed within a furnace. Further details of the experimental setup can be found in [28].

The electrical properties of the SOFC with a room-temperature-sputtered GDC barrier layer described above are characterized in terms of j-V polarization curves and EIS measurements to compare the final cells performances both with usual H_2 and NH_3 feedings. The study was divided into two steps:

- In the first step, we evaluated the performance of the above-described cell fueled by different hydrogen flowrates; the cell was tested at four different working temperatures (800 °C, 750 °C, 700 °C and 650 °C). For each temperature, different H_2 feeding flowrates (3 NmL $min^{-1}cm^{-2}$, 6 NmL $min^{-1}cm^{-2}$, 9 NmL $min^{-1}cm^{-2}$, 12 NmL $min^{-1}cm^{-2}$ and 15 NmL $min^{-1}cm^{-2}$) were considered. The performance of the cell is evaluated by acquiring j-V curves and EIS spectra for each combination of temperature and flowrate feeding.
- In the second step, we evaluate how the performance of the cell changes according to fuel feeding; for each of the above-mentioned working temperatures and H_2 feeding flowrates, the amount of hydrogen is substituted by NH_3 at different percentages (0%, 25%, 50%, 75% and 100%). The complete study is composed of j-V curves acquired for each combination of working temperature, gas flowrate and NH_3%. Moreover, EIS spectra were acquired for each investigated operating condition.

3. Results and Discussion

3.1. Evaluation of Diluted H_2 Feeding Performance

Sputtered barrier layer button SOFC performances were preliminary studied by means of j-V curves and EIS measurements performed at four working temperatures ranging from 800 °C to 650 °C to estimate the SOFC behavior in hydrogen both at usual industrial working temperatures and in the IT range. j-V curves were acquired with a 0.018 A·s^{-1} current ramp, while EIS measurements were carried out superposing a 0.4 A amplitude signal at 0.5 A cm^{-2} fixed current, with frequencies ranging from 0.01 Hz to 10 kHz and gas feeding provided by a mixture of hydrogen and nitrogen; the choice of nitrogen-diluted hydrogen feeding was useful for two reasons: firstly, it allows to better cover the anode area with a lower hydrogen flux; secondly, it allows to take into account the possible effect of N_2 dilution coming from the decomposition of NH_3.

In Table 1, gas dilution parameters are reported.

Table 1. Diluted H_2 + N_2 flowrates: for each temperature, all the reported flowrates were explored.

H_2 (NmL $min^{-1}cm^{-2}$)	N_2 (NmL $min^{-1}cm^{-2}$)
15	5
12	4
9	3
6	2
3	1

In Figure 1, the j-V curves acquired for each parameter combination are displayed.

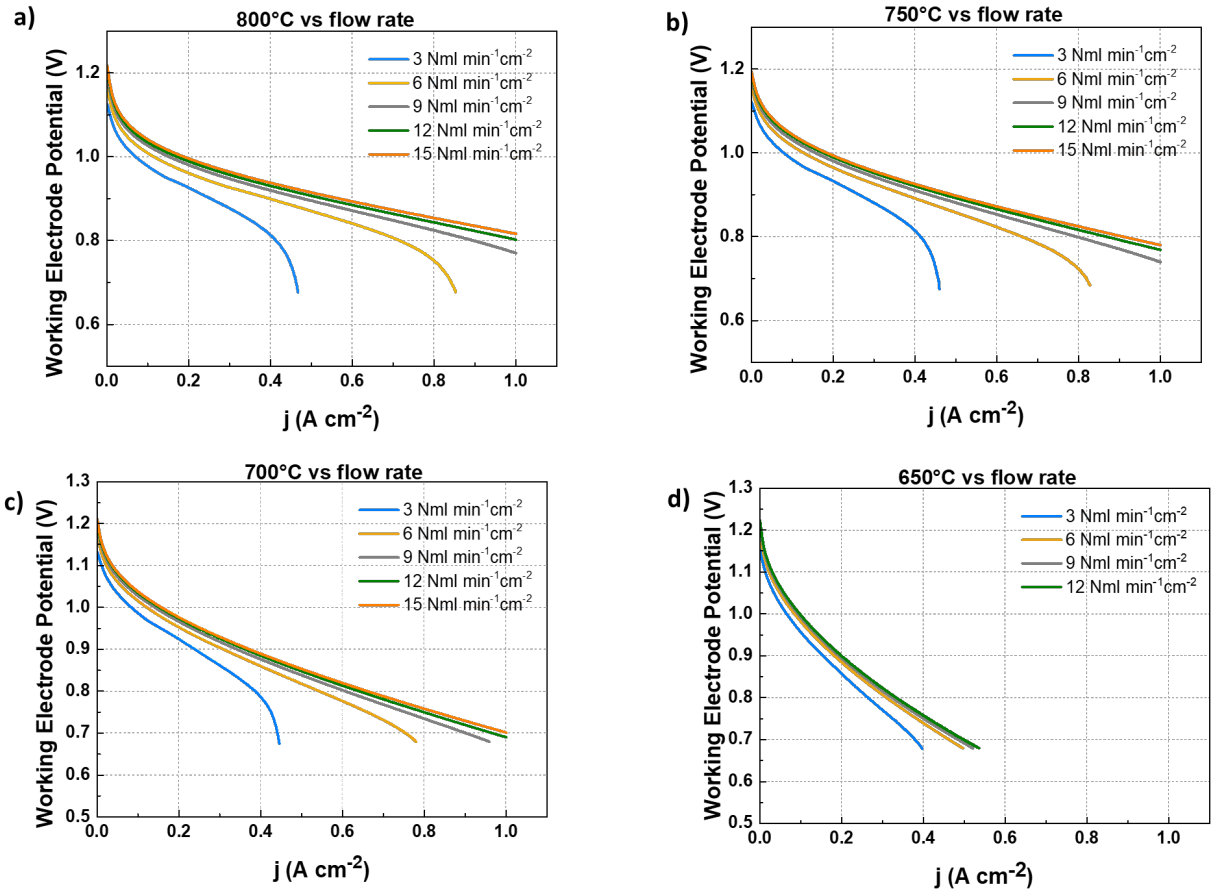

Figure 1. j-V curves acquired at different working temperatures and different diluted hydrogen flowrates (15 NmL·min^{-1}cm^{-2} orange curve, 12 NmL·min^{-1}cm^{-2} green curves, 9 NmL·min^{-1}cm^{-2} gray curves, 6 NmL·min^{-1}cm^{-2} yellow curves and 3 NmL·min^{-1}cm^{-2} blue curves) at 800 °C (**a**), 750 °C (**b**), 700 °C (**c**) and 650 °C (**d**).

From the above Figures (Figure 1a–c), one can see that the sputtered barrier layer SOFCs tested at 800 °C, 750 °C and 700 °C are characterized by no visible limiting current for higher flowrates (i.e., 15 NmL min^{-1}cm^{-2}, 12 NmL min^{-1}cm^{-2} and 9 NmL min^{-1}cm^{-2}), while the change in the slope starts to be visible for 6 NmL min^{-1}cm^{-2} and then becomes evident for the lowest flowrate (3 NmL min^{-1}cm^{-2}), highlighting that for these inlet flowrates, the fuel is consumed faster than it is supplied to the SOFC [29–31]. This effect becomes less evident with decreasing working temperature, with the slopes of the 6 NmL min^{-1}cm^{-2} flowrate curve (yellow line) and 3 NmL min^{-1}cm^{-2} flowrate curve (blue line) becoming less sharp. This is further confirmed by the measurement performed at 650 °C, where the limiting current is not visible anymore for 6 NmL min^{-1}cm^{-2} (yellow curve), and the change in slope for the 3 NmL min^{-1}cm^{-2} is the less pronounced among all the blue curves present in Figure 1. At the lowest working temperature, no measurement was performed at the highest flowrate (i.e., 15 NmL min^{-1}cm^{-2}), because from the data at higher temperatures, the results at 15 NmL min^{-1}cm^{-2} and 12 NmL min^{-1}cm^{-2} are practically the same, without giving additional information on the cell's behavior.

The j-V curves in Figure were used to evaluate the electric efficiency of the cell for each configuration (temperature, H_2 and N_2 content) using the efficiency relation in [1], in which we explicitly report the molar flow $n_{fuel} = \frac{QA_{FC}}{60 \cdot V_m}$ and obtain

$$\eta_{electr} = \frac{60\ V_m VI}{Q\ A_{FC}\ LCV_{H_2}} = 0.664\frac{VI}{Q} = 5.98\frac{Vj}{Q} \quad (1)$$

where LCV_{H_2} is the lower calorific value of H_2 (241,500 J·mol^{-1}), Q is the volumetric flowrate, A_{FC} is the SOFC geometrical area (i.e., 9.08 cm^2) and V_m is the molar volume (i.e., 24,054 NmL·mol^{-1}).

In Figure 2, the evaluated efficiency curves are reported.

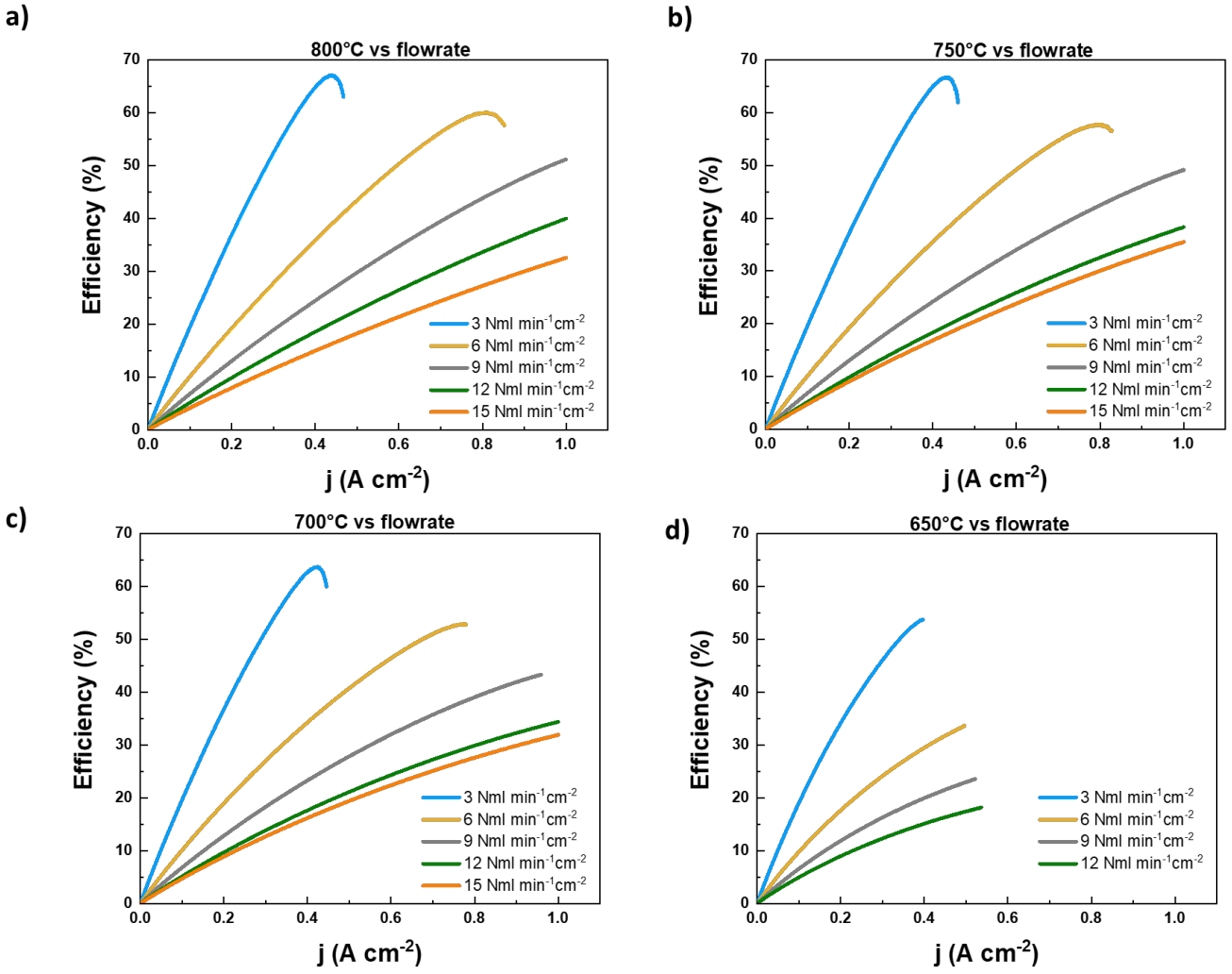

Figure 2. Electric efficiencies evaluated for each working temperature (800 °C (**a**), 750 °C (**b**), 700 °C (**c**) and 650 °C (**d**)) and diluted hydrogen flowrates. The legend present in Figure 2c applies to all the graphs comprising Figure 2.

From Figure 2, it is clear that the electric efficiency lowers with increasing flowrates for all the investigated temperatures and decreases with decreasing working temperatures at fixed inlet flowrate, as expected [2]. Moreover, while an efficiency saturation is clearly visible for the lowest hydrogen flowrates (6 NmL min^{-1}cm^{-2} and 3 NmL min^{-1}cm^{-2}), this saturation starts to disappear at 700 °C for the yellow curve (6 NmL·min^{-1}cm^{-2}) and is completely not visible at 650 °C for both of the lowest flowrates. The highest electrical efficiency (67%) is found at 800 °C and 3 NmL·min^{-1}cm^{-2} flowrate. We point out that the maximum power density achieved is 802 mW·cm^{-2} power density at 1 A cm^{-2} and 12 NmL·min^{-1}cm^{-2} of H_2 at 700 °C. The comparison of these results with those reported in [23,32,33] once again gives evidence of the improved performances in the hydrogen feeding of SOFCs with sputtered GDC barrier layer.

EIS spectra were acquired at 0.5 A cm^{-2} with a superposed perturbation signal of 0.044 A $\cdot cm^{-2}$ amplitude for all the investigated temperatures and flowrates (except for the 3 NmL$\cdot min^{-1}cm^{-2}$ H_2 flowrate that was acquired, the corresponding limiting current being lower than 0.5 A cm^{-2}). In Figure 3, the obtained results are displayed.

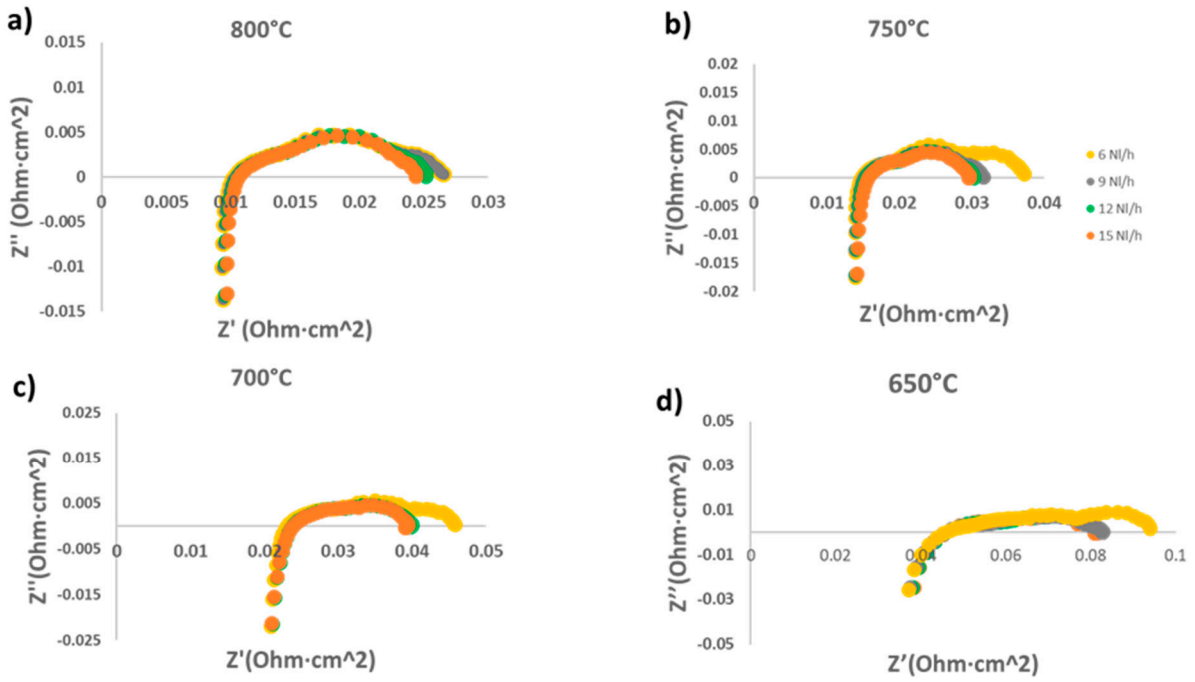

Figure 3. Nyquist plot of EIS measurements performed on the sputtered GDC barrier layer SOFC for each explored temperature (**a**–**d**) and each flowrate: 6 (yellow), 9 (gray), 12 (green) and 15 (orange) NmL$\cdot min^{-1}cm^{-2}$.

Looking at the data shown in Figure 3, we can observe that the ohmic and polarization resistances follow the usual trend found in the literature for SOFCs [23,34,35]. In detail, a change in flowrate does not seem to affect the ohmic resistance, while lowering the operating temperature makes this parameter increase (from 0.01 Ohm$\cdot cm^{-2}$ at 800 °C to 0.045 Ohm$\cdot cm^{-2}$ at 650 °C), and this can be related to an inductive contribution at high frequencies that modifies the shape of the high-frequency arc and the value of the ohmic resistance, especially at lower operating temperatures. On the other hand, the polarization resistance is affected by both temperature and flowrate variations; indeed, for the higher temperatures (800 °C, 750 °C and 700 °C), the polarization resistance increases with decreasing flowrates due to the lower amounts of hydrogen available for the SOFC's main reaction [36,37]. At 650 °C, the polarization resistance shows a remarkable increase, especially in correspondence with 6 NmL$\cdot min^{-1}cm^{-2}$. Furthermore, the effect due to the lack of hydrogen in the reaction zone at low H_2 flowrate is also confirmed by the enhancement of the low-frequency arc related to gas diffusion through the electrodes at 6 NmL$\cdot min^{-1}cm^{-2}$.

The above results for the ohmic and polarization resistances at higher gas flowrates are in complete accordance with what is reported in [23], where a single 35 mm cermet support diameter button cell with a 2 cm diameter screen-printed electrode is tested only for one hydrogen flowrate (16 NmL$\cdot min^{-1}cm^{-2}$). Small deviations in the performances can be attributed to the different size (50 mm in diameter of the cermet support, corresponding to 35 mm diameter of the electrode) of the button cell tested here with respect to the button cells tested in [23]. Indeed, in accordance with the results reported in [26], thickness inhomogeneities in a GDC-sputtered barrier layer affect the final cell performances proportionally to the thickness gradient characterizing the barrier layer on the cell.

3.2. NH_3 Feeding Performance Evaluation

Following the procedure used by Dekker et al. [2], we evaluated the cell behavior for NH_3 feeding at different working temperatures (800 °C, 750 °C, 700 °C and 650 °C) by substituting increasing percentages of NH_3 (25%, 50%, 75% and 100%) for each of the diluted H_2 flowrates (3 NmL·min^{-1}cm^{-2}, 6 NmL·min^{-1}cm^{-2}, 9 NmL·min^{-1}cm^{-2}, 12 NmL·min^{-1}cm^{-2} and 15 NmL·min^{-1}cm^{-2}). By comparing the obtained performance to the performance in diluted H_2 observed in both the same cell and in a 50 mm button cell with screen-printed GDC buffer layer, we show that the cell with sputtered GDC barrier layer presents the same behavior independent of the type of feeding, simultaneously confirming significative performance improvement with respect to industrially prepared button SOFCs.

One of the key points to be taken into account in efficiently fueling SOFCs directly with ammonia is the effectiveness of the cracking reaction of ammonia at the anode side, where two NH_3 molecules split into three H_2 and one N_2 in order to provide H_2 as fuel to the cell. It is already known [3,38,39] that Ni/Al_2O_3 acts as a catalyst in the ammonia cracking reaction, while in [2], Ni/YSZ anodes were also demonstrated to be catalysts in the ammonia cracking reaction; thus, the Ni cermet anode of the SOFC studied here should also catalyze the NH_3 splitting reaction.

When comparing the performance in H_2 and in NH_3, it must be considered that, due to the ammonia decomposition, we have 3 H_2 molecules and 2 NH_3 molecules each; following this rule, we obtain, for example, that 12 NmL·min^{-1}cm^{-2} of hydrogen corresponds to 8 NmL·min^{-1}cm^{-2} of pure ammonia feeding (100% NH_3-diluted hydrogen substitution), 9 NmL·min^{-1}cm^{-2} corresponds to 6 NmL·min^{-1}cm^{-2} of pure ammonia feeding and so on. We remark that this feeding conversion is not able to maintain the same energy content at gas inlets under the assumption of complete ammonia cracking at the anode. Therefore, the following conversion table (Table 2) is used in our measurements.

Table 2. NH_3-substituted percentages of diluted H_2 considering a gas made of 100 NH_3 moles.

Substituted %	NH_3	H_2	N_2
0	0	150	50
25	25	113	38
50	50	75	25
75	75	38	13
100	100	0	0

In Figure 4, we report the j-V curves acquired at 800 °C for each different flowrate (3 NmL·min^{-1}cm^{-2}, 6 NmL·min^{-1}cm^{-2}, 9 NmL·min^{-1}cm^{-2}, 12 NmL·min^{-1}cm^{-2} and 15 NmL·min^{-1}cm^{-2}) and the NH_3 percentage substitution of H_2 starting from 0% NH_3 up to 100% NH_3 feeding.

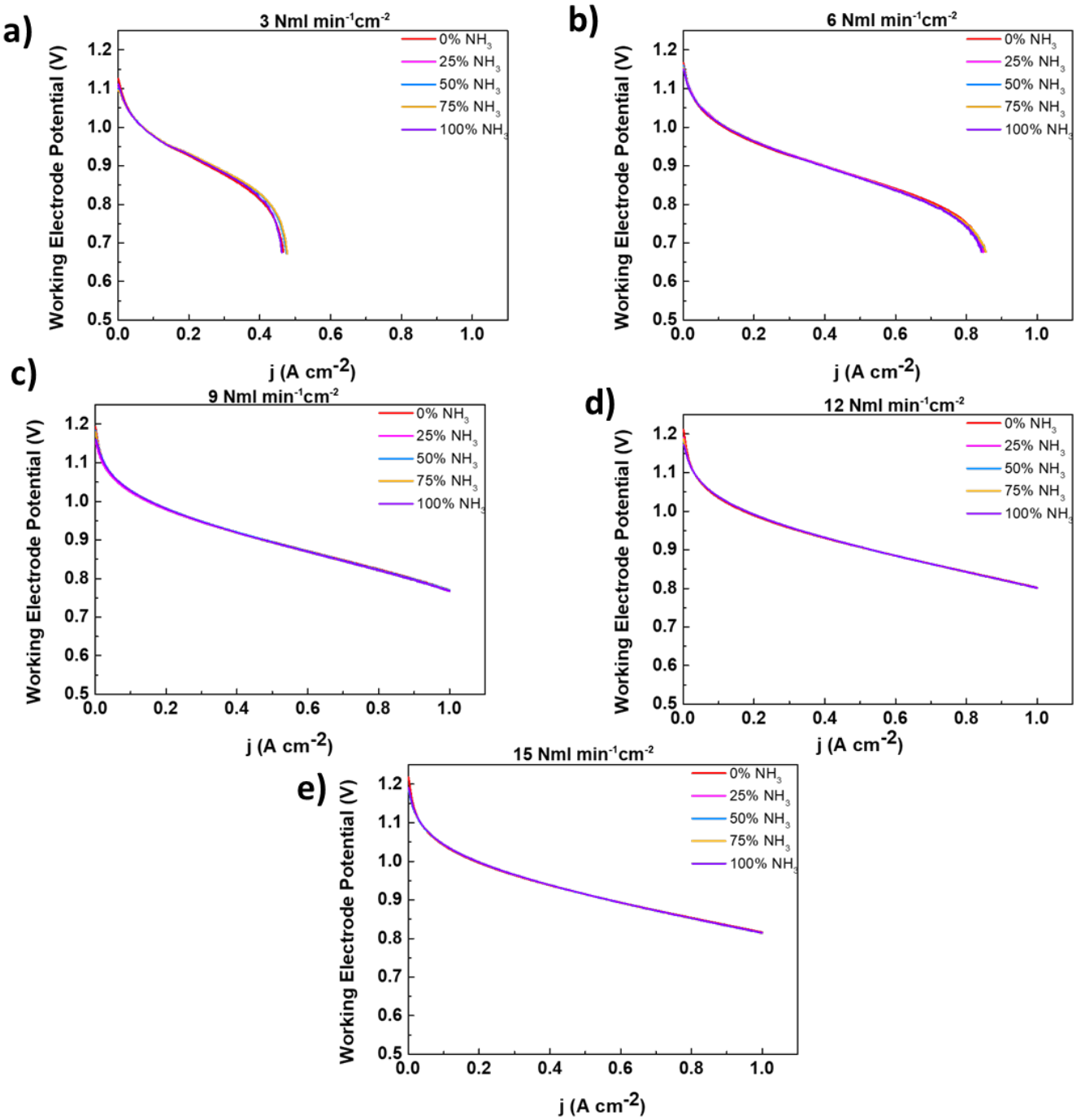

Figure 4. j-V curves acquired at 800 °C at different flowrates: (**a**) 3 NmL· min^{-1}·cm^{-2}, (**b**) 6 NmL· min^{-1}·cm^{-2}, (**c**) 9 NmL· min^{-1}·cm^{-2}, (**d**) 12 NmL· min^{-1}·cm^{-2} and (**e**) 15 NmL· min^{-1}·cm^{-2}; for each flowrate of 0 (red line), 25 (magenta line), 50 (light blue line), 75 (yellow line) and 100 (purple line) %, NH_3 was substituted to diluted hydrogen following the conversion rules resumed in Table 2.

As it is clear in Figure 4, for each initial H_2 flowrate, the corresponding curves with different substituted percentages of NH_3 are perfectly superposed to the 0% substituted one. This means that at 800 °C, the cell does not react to the "change in fuel" and behaves exactly the same in terms of output current when hydrogen is substituted by ammonia. This is not surprising due to the expected 100% cracking reaction efficiency at the anode side at high working temperatures [2]. The same behavior was observed in terms of output

current when performing the same experiment at 750 °C for all the above-presented feeding flowrates and NH_3-substituted percentages.

Once more, given the high performance of sputtered barrier layer SOFCs fed in pure or diluted H_2 (up to ≈ 31% increased performance when compared with SoA button cells with screen-printed GDC layer at 750 °C) [23], the above-mentioned results give further evidence that similar high and promising performances can be achieved by the same SOFC structure fed by ammonia.

In terms of electric conversion efficiencies, the above polarization curves give the results summarized in Figure 5, in which we report the evaluated efficiencies at 6, 9 and 15 NmL·min^{-1}cm^{-2}. In this case, the calculation was performed following Equation (1), taking into account gas percentage substitution A and B:

$$\eta_{electr} = \frac{60\ V_m V I}{Q\ A_{FC}\ \left(A{\cdot}LCV_{H_2} + B{\cdot}LCV_{NH_3}\right)} \quad (2)$$

where LCV_{H_2} and LCV_{NH_3} are the lower calorific values of H_2 (241,500 J·mol^{-1}) and NH_3 (317,000 J·mol^{-1}), respectively, Q is the total volumetric flowrate of the H_2 and NH_3 mixture and A and B are two factors that take into account the gas percentage substitution; therefore, while A assumes the values 1, 0.75, 0.50, 0.25 and 0, B assumes the following values: 0, 0.25, 0.50, 0.75 and 1.

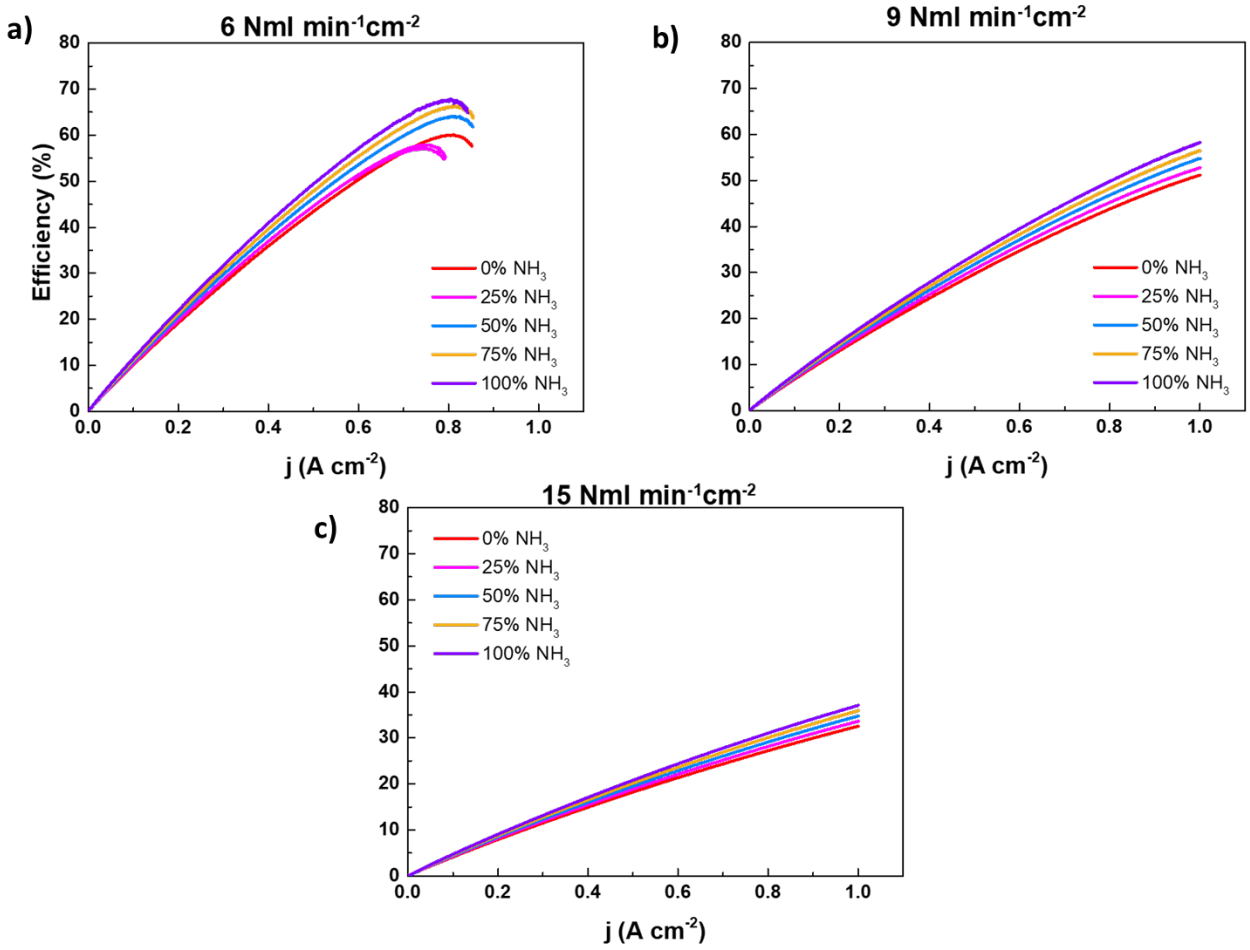

Figure 5. Electric efficiencies evaluated for each total flowrate: (**a**) 6 NmL·min^{-1}cm^{-2}, (**b**) 9 NmL·min^{-1}cm^{-2} and (**c**) 15 NmL·min^{-1}cm^{-2}) as a function of the percentage substitution 0% (red line), 25% (magenta line), 50% (light blue line), 75% (yellow line) and 100% (purple line).

As already seen in Figure 2, the efficiency lowers with increasing flowrates [2]. An efficiency saturation is clearly visible for the lowest hydrogen flowrate (6 NmL·min^{-1}cm^{-2}), disappearing at the highest flowrate of 15 NmL·min^{-1}cm^{-2}. The increase in fuel efficiency with increasing percentage ammonia substitution is due to the higher energy content of ammonia and is in accordance with the results present in [2].

Changes in the electrochemical behavior of SOFC were also monitored by performing EIS measurements at 0% and 100% hydrogen substituted by NH_3 for all the equivalent flowrates and all the operating temperatures. In line with what is presented above, the results in Figure 6 report EIS acquired at 800 °C, because those observed at the different temperatures are practically the same.

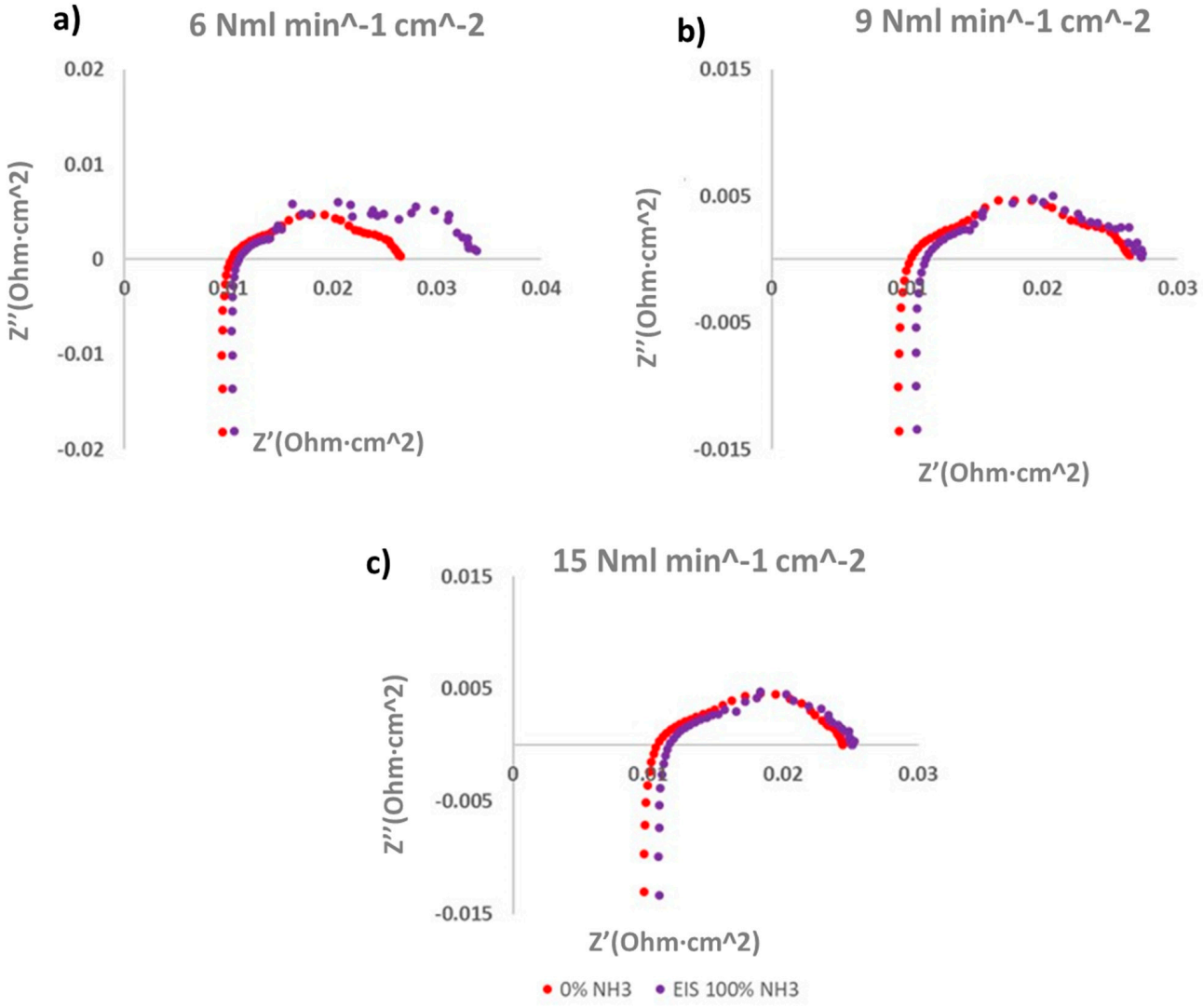

Figure 6. Nyquist plot of EIS measurements performed on the sputtered GDC barrier layer SOFC at 800 °C for 6 NmL·min^{-1}cm^{-2} (**a**), 9 NmL·min^{-1}cm^{-2} (**b**) and 15 NmL·min^{-1}cm^{-2} (**c**) in diluted hydrogen (0% NH_3, red dots) and direct ammonia feeding (100% NH_3, purple dots).

At all the flowrates, the ohmic resistance is always lower when the cell is fed in diluted H_2 (red dots), in agreement with previous results [9], measuring a drop in the open-circuit voltage (OCV) with increasing NH_3 concentrations. Indeed, we observed a similar small drop with increasing ammonia percentage substitutions for all the flowrates in the j-V curves in Figure 4, despite the 100% efficiency of the ammonia cracking reaction. Such a small OCV drop with increasing ammonia concentrations is probably related to the endothermic nature of ammonia dissociation reaction being responsible for slight

temperature decrement when increasing ammonia content. Moreover, the polarization resistance observed at 9 NmL·min^{-1}cm^{-2} and 15 NmL·min^{-1}cm^{-2} slightly decreases in the 100% NH_3 feeding, giving evidence of the decrement in the overpotentials when directly fueling the SOFC with ammonia [9]. Due to unexpected electrical contact problems, the measurement at 6 NmL·min^{-1}cm^{-2} was not carried out.

In the following j-V and efficiency data, since we observed similar curves under higher flowrates (9 NmL·min^{-1}cm^{-2}, 12 NmL·min^{-1}cm^{-2} and 15 NmL·min^{-1}cm^{-2}) and for the lower flowrates (3 NmL·min^{-1}cm^{-2} and 6 NmL·min^{-1}cm^{-2}), we show only one curve for the " high" and "low" flowrate results, these two curves being completely representative of all the measurements performed [2].

At 750 °C, the curves in Figure 7 are almost completely superposed, in particular for the "low" flowrate, indicating the effectiveness of the NH_3 cracking reaction. As already observed for the 800 °C operating temperature, the only change in the j-V curves is given by the slight lowering of the OCV, with increasing ammonia percentage substitution favored by the endothermic cracking reaction. We point out that the same output power density of 802 mW·cm^{-2} at 1 A·cm^{-2} was observed both for 12 NmL·min^{-1}cm^{-2} of H_2 and for the equivalent NH_3 flowrate (100% NH_3-substituted, corresponding to 8 NmL·min^{-1}cm^{-2} of ammonia, according to the conversion in Table 2). These values of the power density outputs are comparable to those obtained in industrial SoA SOFCs with screen-printed GDC fed with higher hydrogen flowrates [23,24].

At 700 °C, the curves in Figure 7 start to spread out for both the "low" and "high" flowrates, probably due to the less effective ammonia cracking reaction at the Ni cermet anode. By the way, the power density lowering with the change in fuel results to be negligible for the "low" flowrate curve (about 2% at 0.4 A·cm^{-2} and 3.6% at maximum current density 0.75 A·cm^{-2}). The "high" flowrate curve shows the same behavior but with a higher reduction in the power density generated by the cell (−3.2% at 0.4 A·cm^{-2} and −6.7% at 0.88 A·cm^{-2}). Therefore, even higher NH_3 substitution percentages are still efficient in terms of the output power density, with values not appreciably different from those obtained in diluted hydrogen at 700 °C.

At 650 °C, as a consequence of the anode's reduced efficiency for the ammonia splitting reaction, both the "low" and "high" flowrate curves show an increased spread as a function of the NH_3 substitution. Indeed, both the displayed curves spread away, with the outlet current decreasing with increasing ammonia substitution. The maximum power density percentage variation is observed between the diluted hydrogen cell and the directly ammonia-fed cell (100% ammonia substituted) at the higher flowrate, −11.5% being the difference in the generated power densities.

In Figure 8, the "low" and "high" fuel–electricity conversion efficiencies are reported as a function of temperature and ammonia percentage substitution.

At 750 °C, it is clear that the efficiency trend and values show the same behavior found at 800 °C. The maximum value is found for the "low" flowrate at 100% substituted ammonia, while the minimum is obtained at 0% substituted ammonia for the "high" flowrate.

At 700 °C, we notice a lowering in the evaluated efficiencies with respect to those observed at 800 and 750 °C. For the "high" flowrate curves related to 25 and 50% substitution, the efficiencies become lower than those acquired in diluted hydrogen (0% substituted), pointing out, again, that at this temperature the cracking reaction at the anode is not 100% efficient anymore.

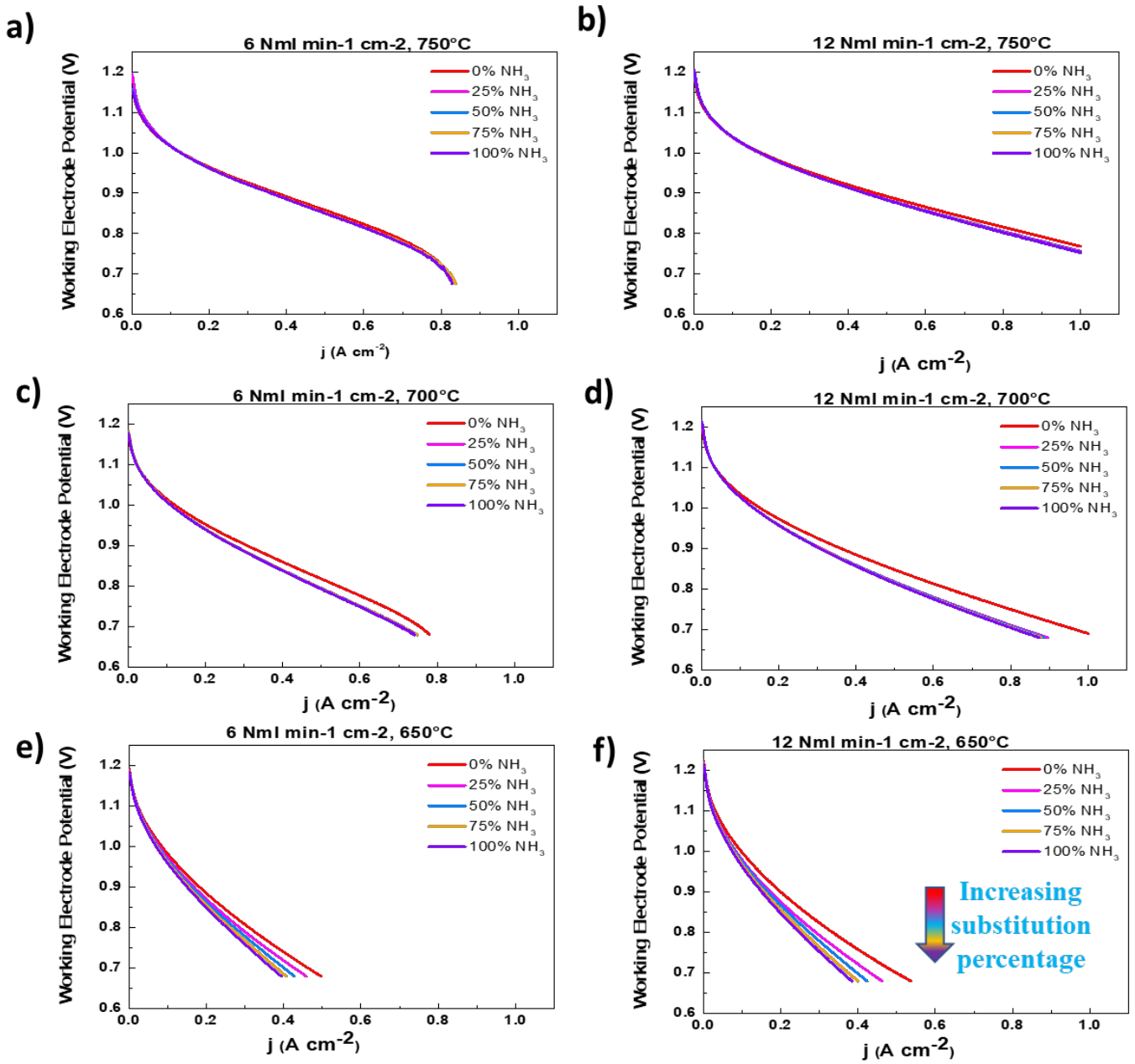

Figure 7. j-V curves acquired at different working temperatures (750 °C in (**a**,**b**), 700 °C in (**c**,**d**) and 650 °C in (**e**,**f**)) for low flowrate (6 NmL·min^{-1}cm^{-2}) and high flowrate (12 NmL·min^{-1}cm^{-2}) and for different percentage substitutions of diluted hydrogen with ammonia: 0% NH_3 (diluted hydrogen, red line), 25% NH_3 (magenta line), 50% NH_3 (light blue line), 75% NH_3 (yellow line) and 100% NH_3 (pure ammonia feeding, purple line).

At 650 °C, the trend observed for higher working temperatures starts to show an inversion. The maximum efficiency is much lower than the values observed before and, more importantly, it is possible to see that at lower substitution percentages, the cell is less efficient compared with the 0% substitution one. This is in agreement with the behavior reported in [18], again due to the temperature-dependent power generation in ammonia-fed cells, strictly related to the catalytic activity of the anode in the cracking reaction. Nonetheless, we point out here that GDC-sputtered barrier layers embedded in SoA industrial SOFCs are able to increase the cell current generation up to +78% at 650 °C and +60% at 700 °C and 800 mV, as reported in [23]. Therefore, comparing the results

obtained with the ones obtained with an SoA button cell with industrially screen-printed barrier layer, we can make the following observation: the output current density produced by sputtered barrier layer button SOFCs fed by 8 NmL·min^{-1}cm^{-2}, pure ammonia at 800 mV and 700 °C (i.e., 0.54 A·cm^{-2}) is exactly the same output current density obtained in an SoA button cell with industrial screen-printed GDC barrier layer fueled with a higher hydrogen flowrate (i.e., 16 NmL·min^{-1}cm^{-2}).

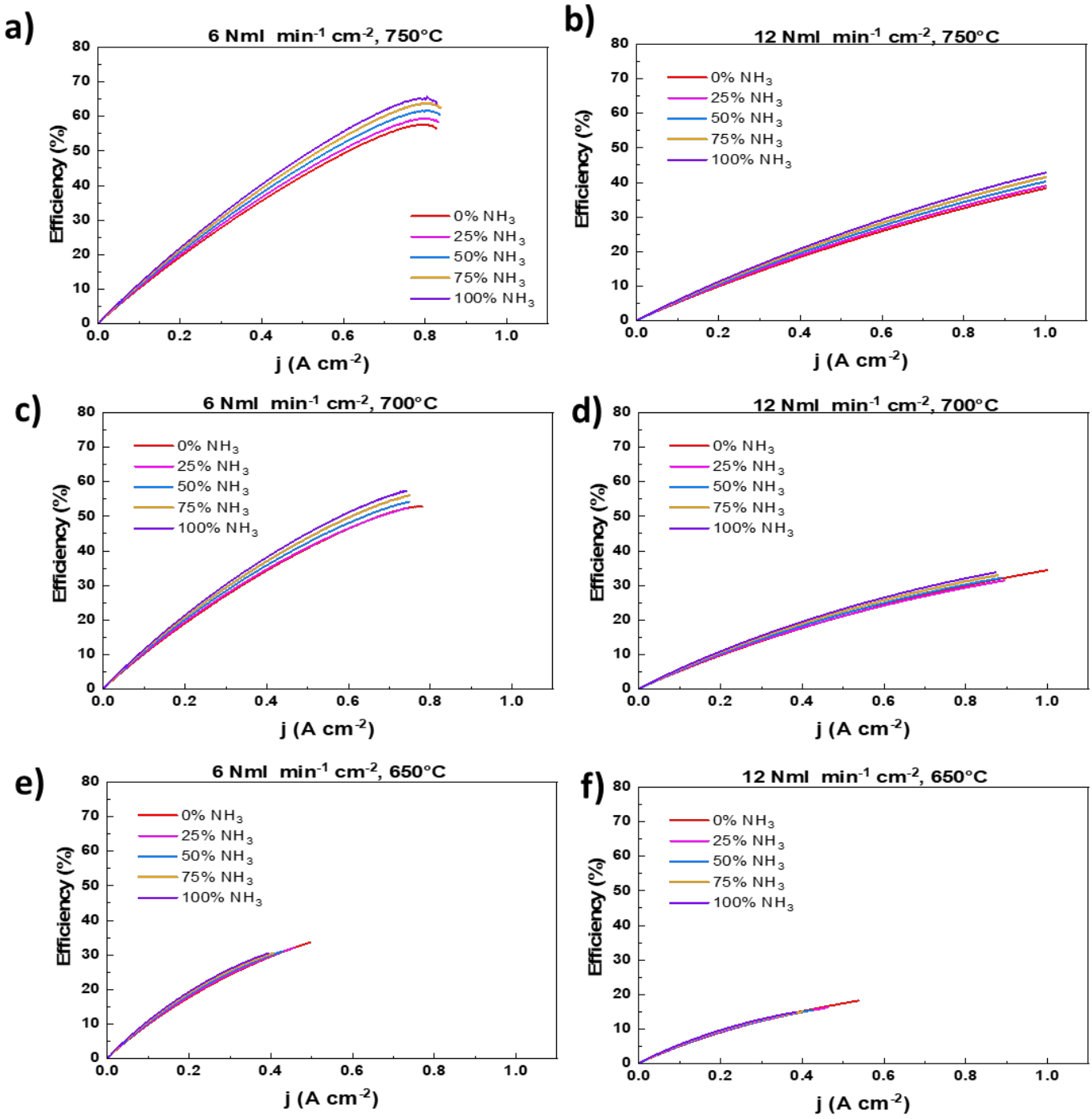

Figure 8. Electrical efficiencies for 750 °C (**a**,**b**), 700 °C (**c**,**d**) and 650 °C (**e**,**f**) operating temperatures and function of high (12 NmL·min^{-1}cm^{-2}) and low (6 NmL·min^{-1}cm^{-2}) flowrates for the different ammonia substitution percentages: 0% (red line), 25% (magenta line), 50% (light blue line), 75% (yellow line) and 100% (purple line).

Finally, all the observations made above are also confirmed by analyzing the Nyquist plots shown in Figure 9.

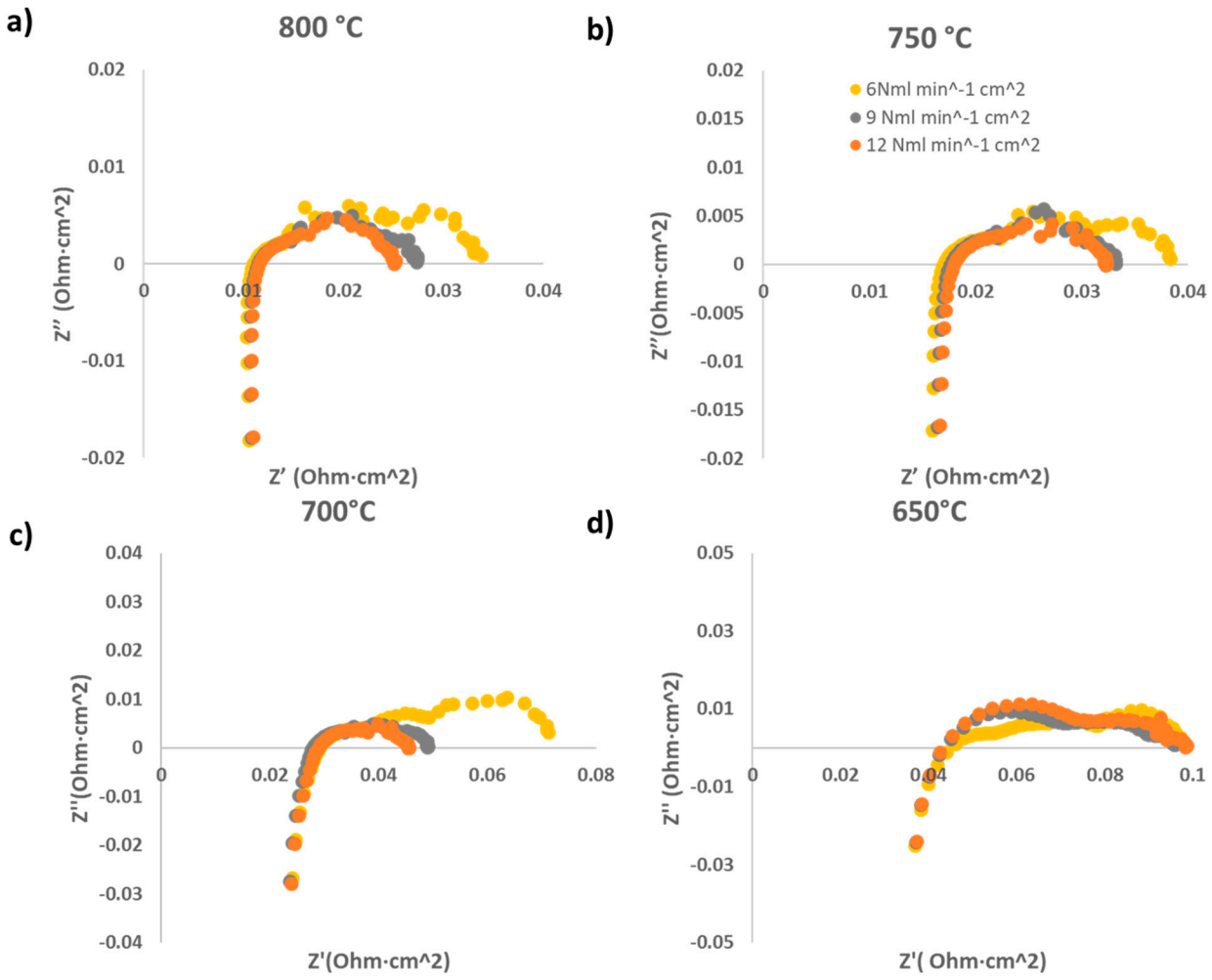

Figure 9. EIS spectra acquired at 800 °C (**a**), 750 °C (**b**), 700 °C (**c**) and 650 °C (**d**) at 6 NmL·min^{-1}cm^{-2} (yellow dots), 9 NmL·min^{-1}cm^{-2} (grey dots) and 12 (orange dots) NmL·min^{-1}cm^{-2} in 100% NH_3 as a function of the total inlet flowrate. The legend present in the graph at 750 °C applies to all the measurements present in the figure.

Figure 9 shows that the polarization and ohmic resistance trends as a function of the inlet flowrate for the two higher operating temperatures are the same as those observed for diluted hydrogen feeding. There is no evidence of ohmic resistance dependence with the ammonia flowrate or of the polarization resistance increasing with decreasing flowrate. These results further confirm that the change in fuel does not affect button cell behavior at high temperatures. At 700 °C, while no ohmic resistance change is observed with respect to the diluted hydrogen feeding (see Figure 3), it is possible to see an increase in the polarization resistance at both the NH_3 equivalent feeding at 6 NmL·min^{-1}cm^{-2} and at 9 NmL·min^{-1}cm^{-2} of diluted hydrogen, providing further evidence of the lack in hydrogen available to sustain the SOFC processes. On the other hand, at 650 °C, we can observe a huge polarization resistance increment for all the reported flowrates, in accordance with the efficiency lowering reported in Figure 8.

4. Conclusions

To compare the performances of SOFCs with sputtered and screen-printed SoA GDC buffer layers, we first performed the electrochemical characterization of a 9 cm^2 active

surface area button cell by fueling it with different hydrogen flowrates (3 NmL·min^{-1}cm^{-2}, 6 NmL·min^{-1}cm^{-2}, 9 NmL·min^{-1}cm^{-2}, 12 NmL·min^{-1}cm^{-2} and 15 NmL·min^{-1}cm^{-2}), varying the working temperatures (800 °C, 750 °C, 700 °C and 650 °C). The performance of the cell was measured acquiring j-V curves and EIS spectra for each combination of temperature and flowrate feeding. Successively, to evaluate how the performance of the cell is changed by the change in fuel, for each of the above-mentioned working temperatures, the amount of hydrogen was substituted by NH_3 at different percentages (0%, 25%, 50%, 75% and 100%). The experimental results, composed of j-V curves acquired for each combination of working temperature, flowrate of the gas feeding and NH_3 percentage substitution, clearly show that for the higher explored working temperatures (800 °C and 750 °C), the power density values do not present any sign of dependence upon the fuel type. Values of 802 mW·cm^{-2} at 1 A·cm^{-2} were found when feeding the cell with both 8 NmL·min^{-1}cm^{-2} of ammonia and with an equivalent flowrate of 12 NmL·min^{-1}cm^{-2} of H_2. At lower working temperatures (700 °C and 650 °C), we measured an output current density value of 0.54 A·cm^{-2} in a pure ammonia flowrate of 12 NmL·min^{-1}cm^{-2}, at 800 mV and 700 °C, equal to the value observed in SoA button cells with an industrial screen-printed GDC barrier layer fueled with 16 NmL·min^{-1}cm^{-2} of H_2. Due to the improved electrochemical performances gained in the case of cells with sputtered GDC thin buffer layers, these power and current density output values are always comparable or even higher than those obtained in industrial SoA SOFCs with screen-printed GDC layers fed with higher hydrogen flowrates. The obtained results indicate that these innovative SOFC structures, preserving the improved electrochemical performances observed in pure H_2 at high temperatures (750–800 °C), are also suitable for use with ammonia fuel. Moreover, the results at low temperatures, thanks to the better performances related to the presence of the sputtered GDC layer, suggest possible applications of these SOFCs fueled by ammonia, even in the so-called Intermediate Temperature (IT) range.

Author Contributions: Conceptualization, B.M. and J.M.; methodology, B.M.; validation, B.M. and J.M.; formal analysis, N.C. and P.P.; investigation, N.C. and B.M.; resources, B.M., J.M., G.C., D.M. and C.P.; data curation, N.C., P.P. and H.S.U.R.; writing—original draft preparation, N.C.; writing—review and editing, L.M., B.M., J.M., A.G., C.P. and P.P.; visualization, N.C.; supervision, L.M., C.P., J.M. and A.G.; project administration, C.P.; funding acquisition, C.P. and L.M. All authors have read and agreed to the published version of the manuscript.

Funding: This research received no external funding.

Data Availability Statement: The data that support the findings of this study are available on request from the corresponding author.

Conflicts of Interest: The authors declare no conflict of interest.

References

1. Hagen, A.; Langnickel, H.; Sun, X. ScienceDirect Operation of solid oxide fuel cells with alternative hydrogen carriers. *Int. J. Hydrogen Energy* **2019**, *44*, 18382–18392. [CrossRef]
2. Dekker, N.J.J.; Rietveld, G. Highly efficient conversion of ammonia in electricity by solid oxide fuel cells. *J. Fuel Cell Sci. Technol.* **2006**, *3*, 499–502. [CrossRef]
3. Lucentini, I.; Garcia, X.; Vendrell, X.; Llorca, J. Review of the Decomposition of Ammonia to Generate Hydrogen. *Ind. Eng. Chem. Res.* **2021**, *60*, 18560–18611. [CrossRef]
4. Humphreys, J.; Lan, R.; Tao, S. Development and Recent Progress on Ammonia Synthesis Catalysts for Haber–Bosch Process. *Adv. Energy Sustain. Res.* **2021**, *2*, 2000043. [CrossRef]
5. Abdelkareem, M.A.; Elsaid, K.; Wilberforce, T.; Kamil, M.; Sayed, E.T.; Olabi, A. Environmental aspects of fuel cells: A review. *Sci. Total Environ.* **2021**, *752*, 141803. [CrossRef]
6. Papurello, D.; Silvestri, S.; Modena, S. Biogas trace compounds impact on high-temperature fuel cells short stack performance. *Int. J. Hydrogen Energy* **2021**, *46*, 8792–8801. [CrossRef]
7. Zhou, J.; Wang, Z.; Han, M.; Sun, Z.; Sun, K. Optimization of a 30 kW SOFC combined heat and power system with different cycles and hydrocarbon fuels. *Int. J. Hydrogen Energy* **2022**, *47*, 4109–4119. [CrossRef]
8. Chen, Z.; Ristig, S.; Poschmann, M.; Folke, J.; Go, O.; Heumann, S.; Ruland, H. Ammonia Decomposition in the Process Chain for a Renewable Hydrogen Supply. *Chem. Ing. Tech.* **2022**, *94*, 1413–1425. [CrossRef]

9. Cinti, G.; Desideri, U.; Penchini, D.; Discepoli, G. Experimental analysis of SOFC fuelled by ammonia. *Fuel Cells* **2014**, *14*, 221–230. [CrossRef]
10. Mukherjee, S.; Devaguptapu, S.V.; Sviripa, A.; Lund, C.R.F.; Wu, G. Low-temperature ammonia decomposition catalysts for hydrogen generation. *Appl. Catal. B Environ.* **2018**, *226*, 162–181. [CrossRef]
11. Hussain, S.; Yangping, L. Review of solid oxide fuel cell materials: Cathode, anode, and electrolyte. *Energy Transit.* **2020**, *4*, 113–126. [CrossRef]
12. Mahato, N.; Banerjee, A.; Gupta, A.; Omar, S.; Balani, K. Progress in material selection for solid oxide fuel cell technology: A review. *Prog. Mater. Sci.* **2015**, *72*, 141–337. [CrossRef]
13. Jacobson, A.J. Materials for solid oxide fuel cells. *Chem. Mater.* **2010**, *22*, 660–674. [CrossRef]
14. Brett, D.J.L.; Atkinson, A.; Brandon, N.P.; Skinner, S.J. Intermediate temperature solid oxide fuel cells. *Chem. Soc. Rev.* **2008**, *37*, 1568–1578. [CrossRef] [PubMed]
15. Solovyev, A.; Shipilova, A.; Smolyanskiy, E.; Rabotkin, S.; Semenov, V. The Properties of Intermediate-Temperature Solid Oxide Fuel Cells with Thin Film Gadolinium-Doped Ceria Electrolyte. *Membranes* **2022**, *12*, 896. [CrossRef]
16. Kwon, C.W.; Son, J.W.; Lee, J.H.; Kim, H.M.; Lee, H.W.; Kim, K.B. High-performance micro-solid oxide fuel cells fabricated on nanoporous anodic aluminum oxide templates. *Adv. Funct. Mater.* **2011**, *21*, 1154–1159. [CrossRef]
17. Solovyev, A.A.; Sochugov, N.S.; Rabotkin, S.V.; Shipilova, A.V.; Ionov, I.V.; Kovalchuk, A.N.; Borduleva, A.O. Application of PVD methods to solid oxide fuel cells. *Appl. Surf. Sci.* **2014**, *310*, 272–277. [CrossRef]
18. Coddet, P.; Liao, H.L.; Coddet, C. A review on high power SOFC electrolyte layer manufacturing using thermal spray and physical vapour deposition technologies. *Adv. Manuf.* **2014**, *2*, 212–221. [CrossRef]
19. Barone, C.; Galdi, A.; Lampis, N.; Maritato, L.; Granozio, F.M.; Pagano, S.; Perna, P.; Radovic, M.; Uccio, U.S. Charge density waves enhance the electronic noise of manganites. *Phys. Rev. B* **2009**, *80*, 115128. [CrossRef]
20. Orgiani, P.; Adamo, C.; Barone, C.; Galdi, A.; Pagano, S.; Petrov, A.Y.; Quaranta, O.; Aruta, C.; Ciancio, R.; Polichetti, M.; et al. Epitaxial growth of $La_{0.7}Ba_{0.3}MnO_3$ thin films on MgO substrates: Structural, magnetic, and transport properties. *J. Appl. Phys.* **2008**, *103*, 093902. [CrossRef]
21. Makous, J.L.; Maritato, L.; Falco, C.M.; Cronin, J.P.; Rajendran, G.P.; Uhlmann, E.V.; Uhlmann, D.R. Superconducting and structural properties of sputtered thin films of $YBa_2Cu_3O_{7-x}$. *Appl. Phys. Lett.* **1987**, *51*, 2164–2166. [CrossRef]
22. Andreone, A.; DiChiara, A.; Peluso, G.; Santoro, M.; Attanasio, C.; Maritato, L.; Vaglio, R. Surface impedance measurements of superconducting (NbTi)N films by a ring microstrip resonator technique. *J. Appl. Phys.* **1993**, *73*, 4500–4506. [CrossRef]
23. Coppola, N.; Polverino, P.; Carapella, G.; Sacco, C.; Galdi, A.; Montinaro, D.; Maritato, L.; Pianese, C. Optimization of the electrical performances in Solid Oxide Fuel Cells with room temperature sputter deposited $Gd_{0.1}ce_{0.9}o_{1.95}$ buffer layers by controlling their granularity via the in-air annealing step. *Int. J. Hydrogen Energy* **2020**, *45*, 12997–13008. [CrossRef]
24. Coppola, N.; Polverino, P.; Carapella, G.; Sacco, C.; Galdi, A.; Ubaldini, A.; Vaiano, V.; Montinaro, D.; Maritato, L.; Pianese, C. Structural and electrical characterization of sputter-deposited $Gd_{0.1}Ce_{0.9}O_{2-\delta}$ thin buffer layers at the Y-stabilized zirconia electrolyte interface for IT-solid oxide cells. *Catalysts* **2018**, *8*, 571. [CrossRef]
25. Coppola, N.; Sami, H.; Rehman, U.; Carapella, G.; Polverino, P.; Montinaro, D.; Martinelli, F.; Granata, V.; Galdi, A.; Maritato, L.; et al. ScienceDirect Large area solid oxide fuel cells with room temperature sputtered barrier layers: Role of the layer thickness and uniformity in the enhancement o f the electrochemical performances and durability. *Int. J. Hydrogen Energy* 2023, *in press*. [CrossRef]
26. Coppola, N.; Polverino, P.; Carapella, G.; Ciancio, R.; Rajak, P.; Montinaro, D.; Martinelli, F.; Maritato, L.; Pianese, C. Large Area Deposition by Radio Frequency Sputtering of $Gd_{0.1}Ce_{0.9}O_{1.95}$ buffer layers in Solid Oxide Fuel Cells: Structural, Morphological and Electrochemical Investigation. *Materials* **2021**, *14*, 5826. [CrossRef]
27. Hagen, A.; Christensen, J.O.; Sudireddy, B.R.; Balomenou, S.; Tsiplakides, D.; Papazisi, K.-M.; Zaravelis, F.; Neofytidis, C.; Ioannidou, E.; Neophytides, S.; et al. Selection of Highlights of the European Project Next Generation Solid Oxide Fuel Cell and Electrolysis Technology—NewSOC. *ECS Trans.* **2021**, *103*, 2205–2216. [CrossRef]
28. Laurencin, J.; Hubert, M.; Sanchez, D.F.; Pylypko, S.; Morales, M.; Morata, A.; Morel, B.; Montinaro, D.; Lefebvre-Joud, F.; Siebert, E. Degradation mechanism of $La_{0.6}Sr_{0.4}Co_{0.2}Fe_{0.8}O_{3-\delta}/Gd_{0.1}Ce_{0.9}O_{2-\delta}$ composite electrode operated under solid oxide electrolysis and fuel cell conditions. *Electrochim. Acta* **2017**, *241*, 459–476. [CrossRef]
29. Fardadi, M.; McLarty, D.F.; Brouwer, J.; Jabbari, F. Enhanced performance of counter flow SOFC with partial internal reformation. *Int. J. Hydrogen Energy* **2014**, *39*, 19753–19766. [CrossRef]
30. Komatsu, Y.; Brus, G.; Kimijima, S.; Szmyd, J.S. The effect of overpotentials on the transient response of the 300W SOFC cell stack voltage. *Appl. Energy* **2014**, *115*, 352–359. [CrossRef]
31. Brus, G.; Miyoshi, K.; Iwai, H.; Saito, M.; Yoshida, H. Change of an anode's microstructure morphology during the fuel starvation of an anode-supported solid oxide fuel cell. *Int. J. Hydrogen Energy* **2015**, *40*, 6927–6934. [CrossRef]
32. Baldi, F.; Wang, L.; Pérez-Fortes, M.; Maréchal, F. A cogeneration system based on solid oxide and proton exchange membrane fuel cells with hybrid storage for off-grid applications. *Front. Energy Res.* **2019**, *6*, 139. [CrossRef]
33. Oryshchyn, D.; Harun, N.F.; Tucker, D.; Bryden, K.M.; Shadle, L. Fuel utilization effects on system efficiency in solid oxide fuel cell gas turbine hybrid systems. *Appl. Energy* **2018**, *228*, 1953–1965. [CrossRef]
34. Yu, H.C.; Zhao, F.; Virkar, A.V.; Fung, K.Z. Electrochemical characterization and performance evaluation of intermediate temperature solid oxide fuel cell with $La_{0.75}Sr_{0.25}CuO_{2.5-\delta}$ cathode. *J. Power Sources* **2005**, *152*, 22–26. [CrossRef]

35. Ahamer, C.; Opitz, A.K.; Rupp, G.M.; Fleig, J. Revisiting the Temperature Dependent Ionic Conductivity of Yttria Stabilized Zirconia (YSZ). *J. Electrochem. Soc.* **2017**, *164*, F790–F803. [CrossRef]
36. Stern, M.; Geary, A.L. Electrochemical Polarization: I. A Theoretical Analysis of the Shape of Polarization Curves. *J. Electrochem. Soc.* **1957**, *104*, 56. [CrossRef]
37. Besghaier, R.; Dhouibi, L.; Jeannin, M.; Safi, M.J. The Synergetic Effect of Flow Velocity and Exposing Time on the Electrochemical Behavior of Cu–Ni 90/10 Alloy in Simulating Conditions of Desalination Plant. *Chem. Africa* **2019**, *2*, 483–495. [CrossRef]
38. Takahashi, A.; Fujitani, T. Kinetic analysis of decomposition of ammonia over Nickel and Ruthenium catalysts. *J. Chem. Eng. Japan* **2016**, *49*, 22–28. [CrossRef]
39. Chellappa, A.S.; Fischer, C.M.; Thomson, W.J. Ammonia decomposition kinetics over Ni-Pt/Al_2O_3 for PEM fuel cell applications. *Appl. Catal. A Gen.* **2002**, *227*, 231–240. [CrossRef]